870 micron observations of nearby 3CRR radio galaxies

A. C. Quillen[1,2,3,4], Jessica Almog[1,5], & Mihoko Yukita[2,6,7]

ABSTRACT

We present submillimeter continuum observations at 870 microns of the cores of low redshift 3CRR radio galaxies, observed at the Heinrich Hertz Submillimeter Telescope. The cores are nearly flat spectrum between the radio and submillimeter which implies that the submillimeter continuum is likely to be synchrotron emission and not thermal emission from dust. The emitted power from nuclei detected at optical wavelengths and in the X-rays is similar in the submillimeter, optical and X-rays. The submillimeter to optical and X-ray power ratios suggest that most of these sources resemble misdirected BL Lac type objects with synchrotron emission peaking at low energies. However we find three exceptions, the FR I galaxy 3C264 and the FR II galaxies 3C390.3 and 3C338 with high X-ray to submillimeter luminosity ratios. These three objects are candidate misdirected high or intermediate energy peaked BL Lac type objects. With additional infrared observations and from archival data, we compile spectral energy distributions (SEDs) for a subset of these objects. The steep dips observed near the optical wavelengths in many of these objects suggest that extinction inhibits the detection and reduces the flux of optical continuum core counterparts. High resolution near or mid-infrared imaging may provide better measurements of the underlying synchrotron emission peak.

Subject headings: galaxies: active

1. Introduction

A snapshot survey of optical counterparts to 3CR radio sources with the Hubble Space Telescope (HST) Wide Field and Planetary Camera 2 (WFPC2) has detected unresolved ($< 0.1''$) optical nuclear components to these luminous radio sources in a large number of objects, particularly at low redshift (Martel et al. 1999; Zirbel & Baum 1998). A correlation between radio core emission

at 5GHz and optical core flux was discovered by (Chiaberge et al. 1999, 2000a; Hardcastle & Worrall 2000), and between the X-ray emission and core radio emission (Hardcastle & Worrall 1999; Canosa et al. 1999) implying that the X-ray and optical emission are relativistically beamed and so probably originate in the radio jet. As pointed out by these studies, these correlations would be consistent with the unifying model that has identified populations of FR I radio sources as BL Lac type objects seen at different viewing angles (Hardcastle et al. 2003; Trussoni et al. 2003; Bai & Lee 2001; Urry & Padovani 1995).

Multiwavelength studies of radio galaxy cores represent a detailed way to test the unification model as their spectral energy distributions (SEDs) can be directly compared to BL Lac type objects. Previous work has focused on three flux points (X-ray, radio and optical) and found that they are not consistent with a single power law (Hardcastle & Worrall 2000), and could be consistent with the SED of a BL Lac type object, but seen at less inclined angles with respect to the line

[1]Department of Physics and Astronomy, University of Rochester, Rochester, NY 14627;

[2]Steward Observatory, The University of Arizona, Tucson, AZ 85721;

[3]Visiting Astronomer at the Infrared Telescope Facility, which is operated by the University of Hawaii under Cooperative Agreement no. NCC 5-538 with the National Aeronautics and Space Administration, Office of Space Science, Planetary Astronomy Program.

[4]*aquillen@pas.rochester.edu*

[5]*jessica_almog@hotmail.com*

[6]Harvard-Smithsonian Center for Astrophysics, 60 Garden Street, Cambridge, MA 02138

[7]*myukita@cfa.harvard.edu*

of sight (Chiaberge et al. 2000a). By carrying out observations of the nuclei in the submillimeter we extend the coverage of the SED to contain a point intermediate between the optical and longer wavelength radio emission. With these additional data we aim to test the hypothesis that the underlying SEDs are similar to BL Lac type objects, estimate the total bolometric output of these nuclei and search for constraints on the shape of the SEDs.

The SEDs of BL Lac type objects and blazars typically have two energy peaks, a lower one from synchrotron radiation and a higher one interpreted to be caused by inverse Compton scattering (e.g., Urry & Padovani 1995; Ghisellini et al. 1988). The previous classification into "low-energy" peaked objects (synchrotron peak residing in the infrared; denoted LBL) and "high-energy" peaked objects (synchrotron residing in the UV/X-rays; denoted HBL) (Padovani& Giommi 1995), has been superseded by a unified continuum where objects exhibit a range of synchrotron peak wavelengths (Fossati et al. 1998; Ghisellini et al. 1988; Padovani et al. 2003; Beckmann et al. 2003).

This calls into question the identification of FR I radio galaxies with LBL BL Lac type objects. Some authors have proposed more complex unification scenarios in which the parent populations of BL Lac type objects include a mix of FR I and FR IIs (Wurtz et al. 1996). Indeed, the extended radio morphologies of BL Lac objects can be of both FR I and II types (e.g., Kollgaard et al. 1996). Thus is more appropriate to unify BL Lac objects more generally with radio galaxies (Rector & Stocke 2001). By studying the nuclear spectral energy distributions of nearby radio galaxies, we aim to find which type of BL Lac type object they would resemble if they were oriented with their jets oriented toward us.

In §2 of this paper we present continuum observations at 870μm of the cores of 34 low redshift radio galaxies. In §3, we explore the luminosity ratios between our data points and those based on core fluxes measured at 5GHz, optical and X-ray wavelengths compiled by previous studies. In §3 we also compile as detailed SEDs of as many objects as possible to see if the SEDs do indeed resemble those of BL Lac type objects and if so which type. A discussion follows in §4.

2. Observations

The 3CRR sample (Laing et al. 1983) is a flux limited sample of the northern sky. It includes all objects with 178MHz flux density greater than 10.9Jy having $\delta > 10°$ and $|b| > 10°$ but excludes the starburst galaxy, M82. In this paper we restrict our study to the low redshift component, $z < 0.1$, of this sample. Many of the galaxies in this subsample have been observed at high angular resolution ($\sim 0.1''$) at visible wavelengths with the Wide Field Planetary Camera 2 (WFPC2) on the Hubble Space Telescope (Martel et al. 1999) and subsequently in the ultraviolet with the STIS NUV MAMA detector (Allen et al. 2002).

We used the Heinrich Hertz Submillimeter Telescope (HHT)[1] (Baars et al. 1999) located on Mt. Graham, Arizona. Observations were carried out 2001 Feb 10-12, with the 19-channel bolometer array which was developed by E. Kreysa and collaborators at the Max-Planck-Institut für Radioastronomie (MPIfR), Bonn (Kreysa et al. 1998). The 19 channels are located in the center and on the sides of two concentric regular hexagons, with an apparent spacing between two adjacent channels (beams) of $50''$. The central frequency of the bolometer is about 345 GHz (the highest sensitivity is reached at 340 GHz), and the instrument is sensitive mainly between 310 and 380 GHz.

To calculate the atmospheric zenith opacity, we made skydip observations every 40 to 80 minutes. During the observations the sky opacity at 345 GHz was around 0.4 most of the time, increasing to 0.9 for a few scans. During the observations, the subreflector was wobbled at 2 Hz in azimuth, with a beam throw of $100''$. Our observation mode consisted of 20 continuum on-off scans, 10 seconds each. Except for the brightest sources, we observed each radio galaxy 6 times in the above mode resulting in a total typical on-source exposure time of 1200 seconds and an actual observing time approximately 3 times this.

For calibration purposes every few hours we also performed mapping and on-off measurements of planets (Venus, Mars). These measurements yielded a conversion factor from observed counts

---

[1]The HHT is operated by the Submillimeter Telescope Observatory on behalf of Steward Observatory and the Max Planck Institut für Radioastronomie.

to mJy/beam of $0.8 - 1.1\,\mathrm{mJy\,beam^{-1}\,count^{-1}}$. The conversion factor is affected by the atmospheric condition during the observations and the uncertainties in the opacity calculation. The pointing of the telescope was checked every few hours. Pointing errors (a few arcseconds) remained well within the beam width $\sim 22\overset{''}{.}7$ throughout these observations.

Data reduction was performed with a customized version of the software package NIC which is part of the GILDAS software package and is a collaborative project of the Centre d'Etudes de Saclay, MPIfR Bonn, the Observatoire de Grenoble and IRAM (Institut de RadioAstronomie Millimétrique). After baseline subtraction and the elimination of spikes in each single coverage, the atmospheric noise, which is highly correlated between the individual channels, was subtracted. The maps were gridded, restored, and finally combined (with an appropriate weighting) into a single map per galaxy. We expected the radio source to be located in the central channel of the array, and for all sources detected this was indeed the case. The flux of the central source was measured using an on-off distance of $120''$ and by subtracting the mean of the sky fluxes from the surrounding channels. For most of the galaxies we had multiple observation sets and the final flux was measured using the noise weighted sum of the flux of the central source in each map.

Of the 46 galaxies from the 3CRR low redshift galaxies observed by Martel et al. (1999), we observed 34 galaxies at the HHT. In addition we include a measurement of the radio galaxy NGC 6251 which has also been observed extensively by HST. NGC 6251 fits the criterion for being selected in the 3CRR galaxy Laing et al. (1983). Of the 35 galaxies observed we detected 24 and estimated 2σ upper limits for the 11 undetected. The measured fluxes and estimated upper limits are listed in Table 1. Observations of three galaxies (3C35, 3C198, 3C227) were repeated during better observing conditions later in the observing run, but remain undetected. These are listed twice in Table 1.

3. Results

For many of these galaxies, nuclear continuum fluxes have been measured in the optical using HST images (Trussoni et al. 2003; Chiaberge et al. 2002b, 1999, 2000a; Hardcastle & Worrall 2000), in the X-rays from Chandar, ROSAT and ASCA data (Hardcastle & Worrall 1999, 2000; Sambruna et al. 1999; Trussoni et al. 2003; Chiaberge et al. 2003; Hardcastle et al. 2001). Using these measured fluxes and 5GHz core fluxes measured by Giovannini et al. (1988); Morganti et al. (1993), we search for correlations and measure spectral indexes between the radio and submillimeter, optical and X-rays. Plots comparing measured core powers are shown in Figure 1. Luminosities have been estimated by $\nu f_\nu 4\pi D^2$ where f_ν is the flux density, ν the frequency and D the distance which we estimate from the redshift using a Hubble constant of 75 km s^{-1} Mpc^{-1}. Spectral indexes for objects detected at 870μm are listed in Table 2 along with luminosities estimated from the submillimeter fluxes. The spectral index, α, is defined in the sense that flux density is proportional to $\nu^{-\alpha}$.

In Figure 1a we see that there is a correlation between the 870μm and 5GHz core luminosities. This implies that the emission at 870μm is not thermal emission from cold dust but more likely to be synchrotron emission. Contamination from $CO(3\text{-}2)$ line emission in the 345 GHz band is unlikely. We find that the typical spectral indexes between the radio (5GHz core) and submillimeter, $\alpha_{sr} \sim 0.2$ This suggests that these sources are approximately flat spectrum up to frequencies higher than 345 GHz.

There is significantly more power emitted from these sources in the submillimeter than at 5GHz. The luminosity ratio between the submillimeter and 5GHz is for the mean approximately 50. This is similar to what is seen in BL Lac type objects which can have their synchrotron emission SED peaking anywhere between the IR through the X-rays (e.g., Fossati et al. 1998; Ghisellini et al. 2002).

From Figures 1b,c we find that the submillimeter luminosities are similar to those emitted in the optical and X-rays. However the scatter in the optical/radio and optical/submillimeter plots is higher than that seen in the submillimeter/radio plots. A large scatter in the optical/submillimeter spectral index, α_{os}, could be caused by a variety of processes including extinction from dust, an additional source of radiation such as continuum emis-

sion from a broad line region, or variations in the position of the emission peaks from an underlying blazar or BL Lac type SED. BL Lac type objects vary in the wavelength position of their synchrotron peaks, and the location of these peaks also depend on orientation angle or beaming. If the underlying SEDs of these sources are similar to blazars or BL Lac type objects we might also expect a large scatter in α_{os} due to differences in synchrotron peak wavelength and orientation angle.

For most of these sources, the luminosity in the submillimeter and the X-rays are similar. Chiaberge et al. (2000b); Trussoni et al. (2003) noted that since the X-ray fluxes are not higher than the optical fluxes, most of these sources are unlikely to be candidate debeamed HBL type objects. However extinction could have reduced the observed optical fluxes. The submillimeter observations have the advantage over the optical ones that they are relatively unaffected by extinction from dust. In Figure 2 we show the X-ray to submillimeter and optical to submillimeter luminosity ratios for objects detected at all three wavelengths. Most of our sources have similar submillimeter and X-ray luminosities, confirming the result by Chiaberge et al. (2000b) that most of these sources are more likely to be similar to LBLs rather than HBLs.

In the subsample containing both X-ray and submillimeter measurements, we find that only 3 objects have X-ray luminosities significantly higher than submillimeter luminosities, the FR I galaxy, 3C264, and the FR II galaxies, 3C382 and 3C390.3. These objects could have SEDs similar to debeamed HBL type objects. We concur with Trussoni et al. (2003) who also found that 3C264 is similar to an HBL. To test this possibility we have plotted on Figure 2 luminosity ratios for debeamed LBL and HBL objects at different orientation angles, based on Mkn421 (dotted line) as done by Chiaberge et al. (2000a) and the means of the populations measured by (Fossati et al. 1998) based on the X-ray selected Einstein Slew BL Lac sample (primarily HBLs), the Wall & Peacock flat spectrum radio quasar sample and the 1Jy BL Lac sample consisting primarily of LBLs. As these BL Lac type objects are debeamed (oriented closer to perpendicular to the line of sight) the optical to submillimeter ratio increases so the

rightmost end of these lines are the objects oriented nearly perpendicular to the line of sight.

Most of 3CRR sources lie in the region expected for LBLs at a range of orientation angles, excepting the three extreme objects 3C264, 3C382 and 3C390.3. A correction for extinction from dust and photoelectric absorption in the X-rays would increase the underlying optical and X-ray fluxes moving the data points upward and to the right in the plot. Consequently some of the sources with low X-ray to submillimeter luminosity ratios could be similar to objects intermediate to LBLs and HBLs. However the three extreme galaxies are unlikely to resemble LBLs and so are candidate HBLs or intermediate objects.

In some cases we have additional information on the object's orientation. Most but not all of FR Is have disks nearly perpendicular to the line of sight and so are likely to be debeamed compared to BL Lac type objects. Those that contains optical jets or exhibit circular dusty disk (such as 3C78 and 3C264) are unlikely to have jets oriented perpendicular to the line of sight (Sparks et al. 2000).

3C264 is probably closer to face on rather than edge-on because it exhibits a nearly round dusty disk, seen in absorption at optical wavelengths (Sparks et al. 2000). 3C390.3 exhibits superluminal motion (Alef et al. 1996), and the jets of 3C382 and 3C390.3 are one sided (Black et al. 1992; Leahy & Perley 1995; Giovannini et al. 2001) suggesting that these two objects are also oriented at high inclination angles to the line of sight. The candidate HBLs we have identified are probably not oriented perpendicular to the line of sight. While 3C390.3 falls near the expected location of the X-ray selected HBL sample, 3C382 and 3C264 are more likely to be similar to intermediate type objects, consistent with recently identified BL Lac populations with spectra in between those of LBLs and HBLs (e.g., Beckmann et al. 2003; Fossati et al. 1998).

3.1. Spectral Energy Distributions

It is clear from the previous section that the possibility of extinction in the optical bands causes an uncertainty which inhibits our study of the underlying SEDs. Because the SEDs of BL Lac type objects are smooth, the spectral indexes are only weakly dependent upon the boosting factor (e.g.,

Chiaberge et al. 2000b). This presents a possible way to tell the difference between obscuration by dust and beaming. If the SED is rapidly changing between the optical and UV wavelengths then it is likely that dust is causing significant obscuration resulting an underestimate of underlying synchrotron emission in the optical region.

If dust is indeed a factor causing us to underestimate the extent of the emission in the optical region then some of these source might be much brighter in the near-IR. Unfortunately only a few of these galaxies were observed by NICMOS. Capetti et al. (2000) found that the SED of 3C264 between 1-2 microns was nearly flat, whereas that of 3C270 decreased remarkably toward shorter wavelengths. Here we compile the SEDs of the objects which were observed at more than one wavelength to examine the shape of the SED in more detail than presented by Capetti et al. (2000); Trussoni et al. (2003). We have compiled in Table 3 core fluxes in the UV and optical from STIS and WFPC2 images, in the near-infrared with NICMOS images (on board HST) , in the mid-infrared from ISOCAM/ISO images and at $3\mu m$ from ground based images taken by us at the IRTF. We have also included measurements by and compiled by Chiaberge et al. (2002a,b); Trussoni et al. (2003).

In Figures 3, and 4 we show the compiled SEDs for FR Is and FR IIs respectively. These are an improvement on previous studies such as Capetti et al. (2002); Trussoni et al. (2003) which contained fewer data points. NGC 4261, and NGC 6251, have notable nearly edge-on dusty disks seen in HST images, and they both have extremely steep SEDs between the near-infrared and optical region, as previous studies have noted (Ferrarese & Ford 1999; Chiaberge et al. 2003). Non-thermal processes such as synchrotron radiation seldom permit extremely sharp drops in a spectral energy distribution. Variability could cause some of the scatter among the points in Figures 3, and 4, however it would not systematically account for a steep drop between the near-infrared and UV wavelengths which is seen in many of these objects. It would be difficult to construct a model from non-thermal emission processes alone in which a number of objects are likely to exhibit such a steep drop exactly in the near-IR/optical region. However extinction by dust naturally causes a steep drop in this region. If we assume that the underlying SED is fairly flat in terms of luminosity, then extinction causes a reduction in the optical flux by more than a factor of 10 in NGC 4261 and by a factor of a few in NGC 6251. We suspect that extinction from dust is important even though many of these radio galaxies were detected as unresolved sources in optical images.

If extinction by dust does affect the detection of unresolved nuclei in the radio galaxies, we expect that subsequent surveys will detect more nuclear sources in the infrared than previous detected in optical surveys. The energy absorbed by the dust should be re-emitted in the infrared, so some of the mid-IR emission should be from hot dust. If we corrected the optical fluxes for extinction, the underlying SED should have more optical emission and consequently lower optical/X-ray and optical/submillimeter spectral indexes. The shape of the SEDs displaying sharp drops between the near-infrared and UV could still be consistent with those of misdirected LBL type objects.

4. Summary and Discussion

In this paper we have presented a survey of submillimeter continuum observations at 870 microns of the low redshift 3CRR radio galaxies, which we observed with the Heinrich Hertz Submillimeter Telescope. We find that the submillimeter luminosities are about 50 times larger than that from the core 5GHz, but similar in size to the X-ray and optical luminosities. The SEDs for most of the FR Is are similar to what is expected from debeamed low energy peaked BL Lac type objects, agreeing with the results of previous works (Chiaberge et al. 2000b; Trussoni et al. 2003). We predict that the SEDs of most of these objects should peak in the infrared and so can be detected with forthcoming mid-IR imaging studies.

By examining a few SEDs in detail we have found good evidence for extinction in the optical region in sources with edge-on disks (M84, NGC 4261, NGC 6251) but not in a source with a face-on disk (3C264). We suspect that some of the scatter in optical spectral indexes is due to extinction from dust, and that many of these nuclei should be brighter at near and mid-infrared wavelengths.

The ratio of submillimeter to X-ray and optical luminosities suggest that most of our sources have

underlying spectra similar to LBL BL Lac type objects. However three objects (the FR I galaxy 3C264, and the FR II galaxies 3C390.3 and 3C382) stand out as having higher optical to submillimeter and X-ray to submillimeter luminosity rations. These three cores are candidate HBL or intermediate type BL Lac type objects.

Previous studies have found that the optical emission is enhanced in some FR II galaxies (e.g., Chiaberge et al. 2002a), suggesting that the optical emission in some cases arises from an additional component such as an accretion disk. The two FR IIs with high optical to submillimeter luminosity ratios in our sample also have high X-ray to submillimeter ratios. This suggests that a similar emission mechanism is responsible for both excesses. One explanation would be that some FR II galaxies have SEDs similar to HBLs rather than LBLs, in which case the emission from the radio to the X-ray would be synchrotron emission. We find only 1 FR I with an HBL type SED whereas we have found 2 such FR IIs out of a smaller number of sources. The larger number of FR IIs is surprising since the unified model for BL Lacs by Fossati et al. (1998); Ghisellini et al. (1988) suggests that those objects with higher luminosities have lower energy synchrotron peaks, whereas FR II radio galaxies tend to have have higher luminosities than FR I radio galaxies.

Another possibility is that an additional emission mechanism is present in both the optical and X-ray wavelengths in 3C390.3 and 3C382. These FR IIs have been identified optically as broad line radio galaxies (BLRGs). Recent work has found that the X-ray to radio ratios in BLRGs quasars tend to be above that expected from an extrapolation of lower energy objects (Hardcastle & Worrall 1999), suggesting that there could be an additional component associated with an accretion disk accounting for the high optical to submillimter and X-ray to submillimeter flux ratios of 3C390.3 and 3C382. FR IIs with weak and strong emission lines may participate differently in unified schemes; it may be predominantly weak-lined FR IIs that are the parent population of BL Lac objects (Hardcastle et al. 1998; Willott et al. 2000).

Recent work on BL Lacs suggest that the SED depends on a beaming factor as well as the energy density in the plasma (Ghisellini et al. 2002). Fossati et al. (1998); Ghisellini et al. (1988, 2002)

found that higher luminosity BL Lac type objects tend to have lower energy synchrotron peaks. However, the objects considered here with likely synchrotron peaks in the infrared have significantly lower power than the BL Lac type objects studied by Fossati et al. (1998). This makes it difficult to unify the 3CRR sample with the known BL Lac population, however as pointed out by Chiaberge et al. (2000a); Trussoni et al. (2003) if the jets contain material accelerated at different velocities then it may be possible to resolve this problem.

The SEDs presented in this paper suffer from lack of infrared coverage, diverse (non-uniform) types of measurements, and are comprised of observations spanning many years. Since these sources are variable, much of the scatter in the points shown could be caused by intrinsic variability. It is likely that the shape of the SED depends on the current luminosity of the source (Vagnetti et al. 2003), an effect that would be difficult to see given the scatter caused by the comparison of points at different epochs. Better wavelength coverage, simultaneous observations and more uniform samples would better allow better studies and tests of unification models.

REFERENCES

Alef, W., Wu, S. Y., Preuss, E., Kellermann, K. I., & Qiu, Y. H. 1996, A&A, 308, 376

Allen, M. G., et al. 2002, ApJS, 139, 411

Alonso-Herrero, A., Quillen, A. C., Rieke, G. H., Ivanov, V. D., & Efstathiou, A. 2003, AJ, 126, 81

Baars, J. W. M., Martin, R. N., Mangum J. G., McMullin, J. P., & Peters, W. L. 1999, PASP, 111, 627

Bai, J. M., & Lee, M. G. 2001, ApJ, 548, 244

Beckmann, V., Engels, D., Bade, N., & Wucknitz, O. 2003, A&A, 401, 927

Black, A. R. S., Baum, S. A., Leahy, J. P., Perley, R. A., Riley, J. M., & Scheuer, P. A. G. 1992, MNRAS, 256, 186

Bower, G. A., et al. 2000, ApJ, 534, 189

Capetti, A., Trussoni, E., Celotti, A., Feretti, L., & Chiaberge, M. 2000, MNRAS, 318, 493

Capetti, A., Trussoni, E., Celotti, A., Feretti, L., & Chiaberge, M. 2002, New Astronomy Reviews, 45, 335

Canosa, C. M., Worrall, D. M., Hardcastle, M. J., & Birkinshaw, M. 1999, MNRAS, 310, 30

Chiaberge, M., Capetti, A., & Celotti, A. 1999, A&A, 349, 77

Chiaberge, M., Capetti, A., & Celotti, A. 2000, A&A, 355, 873

Chiaberge, M., Celotti, A., Capetti, A., & Ghisellini, G. 2000, A&A, 358, 104

Chiaberge, M., Capetti, A., Celotti, A. 2002, A&A, 394, 791

Chiaberge, M., Macchetto, F. D., Sparks, W. B., Capetti, A., Allen, M. G., & Martel, A. R. 2002, ApJ, 571, 247

Chiaberge, M., Gilli, R., Macchetto, F. D., Sparks, W. B., & Capetti, A. 2003, ApJ, 582, 645

Dhawan, V., Kellerman, K. I., & Romney, J. D. 1998, ApJ, 498, L111

Faranoff, B. L., & Riley, J. M. 1974, MNRAS, 167, 31P

Ferrarese, L. & Ford, H. C. 1999, ApJ, 515, 583

Fossati, G., Maraschi, L., Celotti, A., Comastri, A., & Ghisellini, G. 1998, MNRAS, 299, 433

Gavazzi, G., Perol, G. C., & Jaffe, W. 1981, A&A, 103, 35

Ghisellini, G., Celotti, A., Fossati, G., Maraschi, L., & Comastri, A. 1998, MNRAS, 301, 451

Ghisellini, G., Celotti, A., & Costamante, L. 2002, A&A, 386, 833

Giovannini, G., Cotton, W. D., Feretti, L., Lara, L., & Venturi, T. 2001, ApJ, 552, 508

Giovannini, G., Cotton, W. D., Feretti, L., Lara, L., & Venturi, T. 1998, ApJ, 493, 632

Giovannini, G., Feretti, L, Gregorini, L., Parma, P. 1988, A&A, 199, 73

Hardcastle, M. J. & Alexander, P., Pooley, G. G., & Riley, J. M. 1999, MNRAS, 296, 445

Hardcastle, M. J. & Worrall, D. M. 1999, MNRAS, 309, 969

Hardcastle, M. J. & Worrall, D. M. 2000, MNRAS, 314, 359

Hardcastle, M. J., Birkinshaw, M., & Worrall, D. M. 2001, MNRAS, 326, 1499

Hardcastle, M. J., Worrall, D. M., Birkinshaw, M., & Canosa, C. M. 2003, MNRAS, 338, 176

Kollgaard, R. I., Palma, C., Laurent-Muehleisen, S. A., & Feigelson, E. D. 1996, ApJ, 465, 115

Irwin, J. A., Stil, J. M., & Bridges, T. J. 2001, MNRAS, 328, 359

Jones, D. L., Terzian, Y.,& Sramek, R. A. 1981, ApJ, 246, 28

Jones, D. L., Wehrle, A. E. 1997, ApJ, 484, 186

Jones, D. L., Wehrle, A. E., Meier, D. L., Piner, B. G. 2000, ApJ, 534, 165

Jones, D. L. et al. 1986, ApJ, 305, 684

7

Kreysa, E., Gemuend, H. -P., Gromke, J., Haslam, C. G., Reichertz, L., Haller, E. E., Beeman, J. W., Hansen, V., Sievers, A., & Zylka, R. 1998 Proc. SPIE Vol. 3357, Advanced Technology MMW, Radio, and Terahertz Telescopes, ed. T. G. Phillips, p. 319-325

Laing, R. A., Riley, J. M., & Longair, M. S. 1983, MNRAS, 204, 151

Lara, L., Cotton, W. D., Feretti, L., Giovannini, G., Venturi, T., & Marcaide, J. M. 1997, ApJ, 474, 179

Leahy, J. P., & Perley, R. A. 1995, MNRAS, 277, 1097

Leeuw, L. L., Sansom, A. E., Robson, E. I. 2000, MNRAS, 311, 683

Martel, A. R. et al. 1999, ApJS, 122, 81

Morganti, R., Killeen, N. E. B., & Tadhunter, C. N. 1993, MNRAS, 263, 1023

Padovani, P., & Giommi, P. 1995, ApJ, 444, 567

Padovani, P., Perlman, E. S., Landt, H., Giommi, P., & Perri, M. 2003, ApJ, 588, 128

Rector, T. A., & Stocke, J. T. 2001, AJ, 122, 565

Saikia, D. J., Subrahmanya, C. R., Patnaik, A. R., Unger, S. W., Cornwell, T. J., Graham, D. A., & Prabhu, T. P. 1986, MNRAS, 219, 545

Sambruna, R. M., Eracleus, M., & Mushotsky, R. F. 1999, ApJ, 526, 60

Sparks, W. B., Baum, S. A., Biretta, J., Macchetto, F. D., & Martel, A. R. 2000, ApJ, 542, 667

Trussoni, E., Capetti, A., Celotti, A., Chiaberge, M., & Feretti, L. 2003, A&A, 403, 889

Urry, C. M., & Padovani, P. 1995, PASP, 107, 803

Vagnetti, F., Trevese, D., & Nesci, R. 2003, ApJ, 590, 123

Venturi, T., et al. 1995, ApJ, 454, 735

Willott, C. J., Rawlings, S., Blundell, K. M., & Lacy, M. 2000, MNRAS, 316, 449

Wurtz, R., Stocke, J. T., & Yee, H. K. C. 1996, ApJS, 103, 109

Xu, C., Baum, S. A., O'Dea, C. P., Wrobel, J. M., & Condon, J. J. 2000, AJ, 120, 2950

Zirbel, E. L., & Baum, S. A. 1998, ApJS, 114, 177
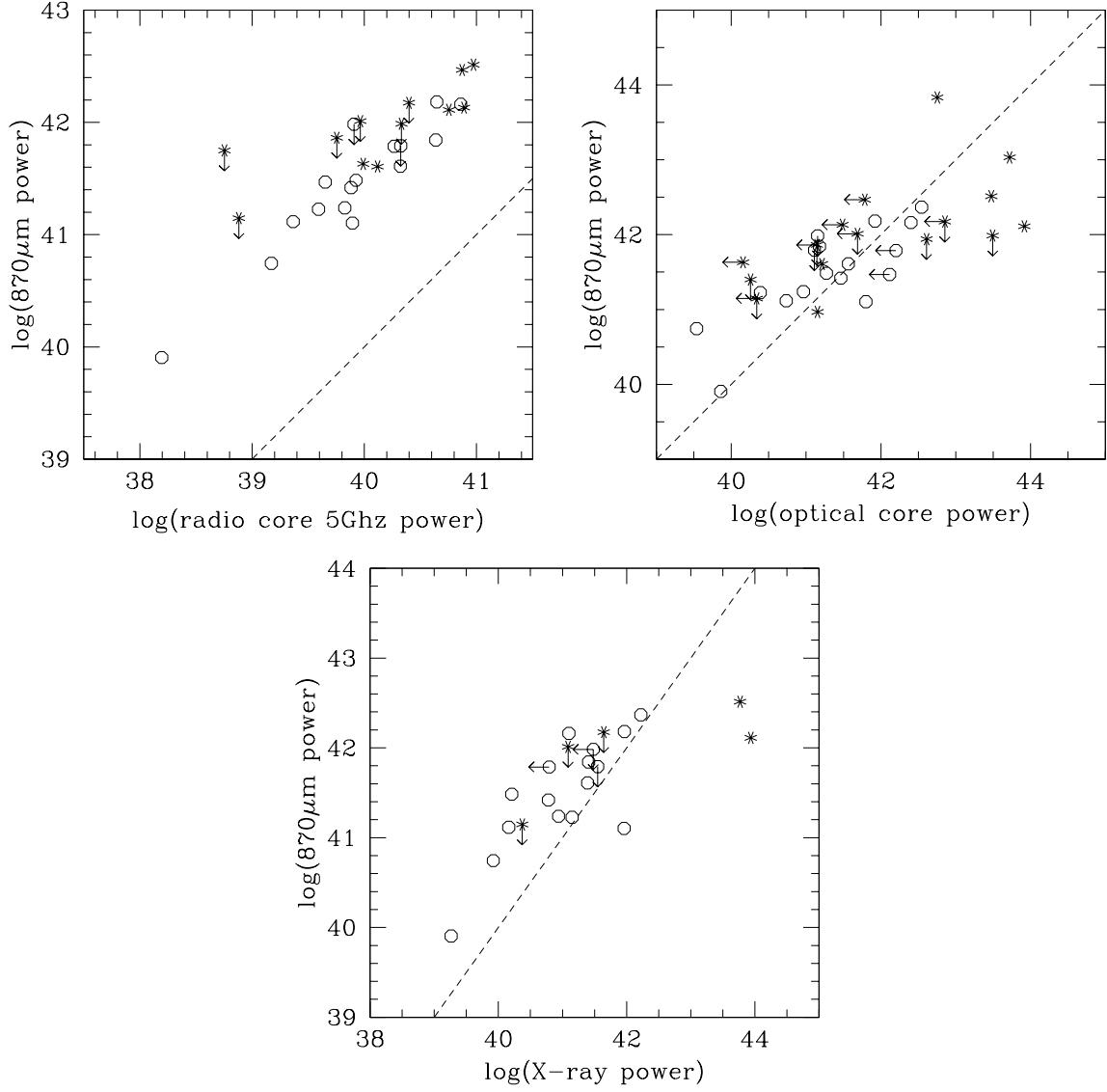
Fig. 1.— A comparison of the power emitted at different wavelengths. a) Comparison between the core power emitted at 5GHz and that emitted in the submillimeter at 345 GHz. FR I's are shown as open circles and FR II's as stars. The log of the luminosities in ergs s^{-1}, (estimated by νL_ν) are shown. The dashed line shows $\alpha = 1$ where the flux $S_\nu \propto \nu^{-\alpha}$, which corresponds to a power νL_ν independent of ν. The luminosity is the same at the two frequencies for points on this line. The submillimeter powers are about 50 times larger than those at 5GHz. Radio 5GHz core fluxes are those measured by (Morganti et al. 1993; Giovannini et al. 1988). b) Comparison between optical and submillimeter power. c) Comparison between X-ray and submillimeter power. Optical points are taken from those compiled and measured by (Trussoni et al. 2003; Chiaberge et al. 2002b, 1999, 2000a; Hardcastle & Worrall 2000), those in the X-rays by (Hardcastle & Worrall 1999, 2000; Sambruna et al. 1999; Trussoni et al. 2003; Chiaberge et al. 2003; Hardcastle et al. 2001). As noted by previous studies (e.g., Chiaberge et al. 2000a), some FR II galaxies have excess optical or X-ray power compared to their radio power. Here we find that the same is true for the optical or X-ray power compared to that emitted in the submillimeter.

9
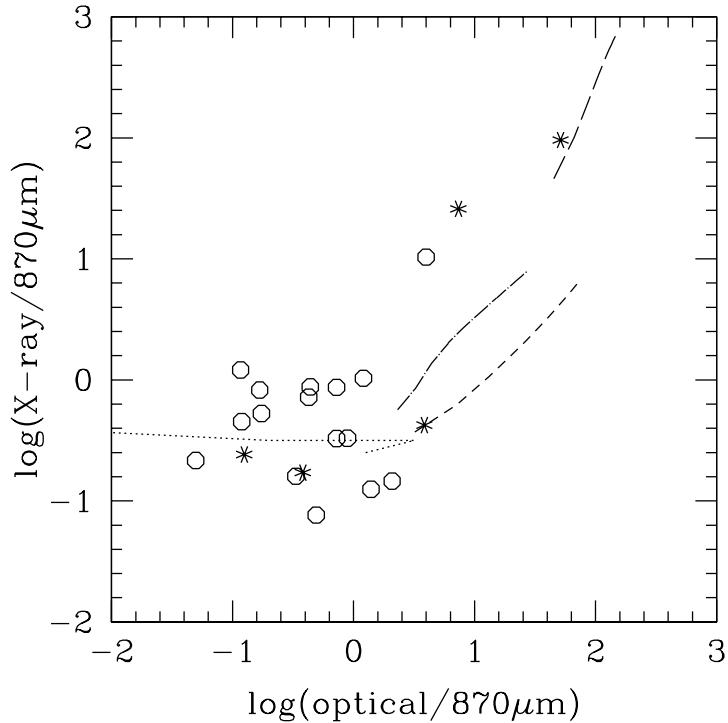
Fig. 2.— Comparison between the ratio of power emitted in X-ray to submillimeter and the ratio of power emitted in optical to submillimeter. FR I's are shown as open circles and FR II's as stars. The FR I with the large X-ray/870μm luminosity ratio is 3C264. The FR IIs on the upper right are 3C390.3 and 3C338. Also shown are the expected ratios for debeamed BL Lac type objects. The dotted line shows that expected for an LBL (based on the spectrum of Mkn421 as done by Chiaberge et al. 2000a). The dashed line shows that based on the mean of the LBL dominated 1Jy radio selected BL Lac sample measured by Fossati et al. (1998) in their Table 5. The leftmost point on the line corresponds to that of the observed BL Lac sample and the rightmost point in the line refers to a debeamed object at an orientation angle of $60°$ assuming $\gamma = 20$. The dashed line shows that based on the mean of the X-ray selected Einstein Slew sample (HBL dominated) as measured by Fossati et al. (1998). The dot dashed line shows that based on the mean of the Wall & Peacock flat spectrum radio quasar sample as measured by Fossati et al. (1998). The objects 3C264, 3C390.3 and 3C338 are candidate low luminosity HBLs. The remaining objects are consistent with LBLs at a range of beaming angles. If dust affects the optical luminosity of the core emission then the true location of the synchrotron components would be further to the right on this plot.
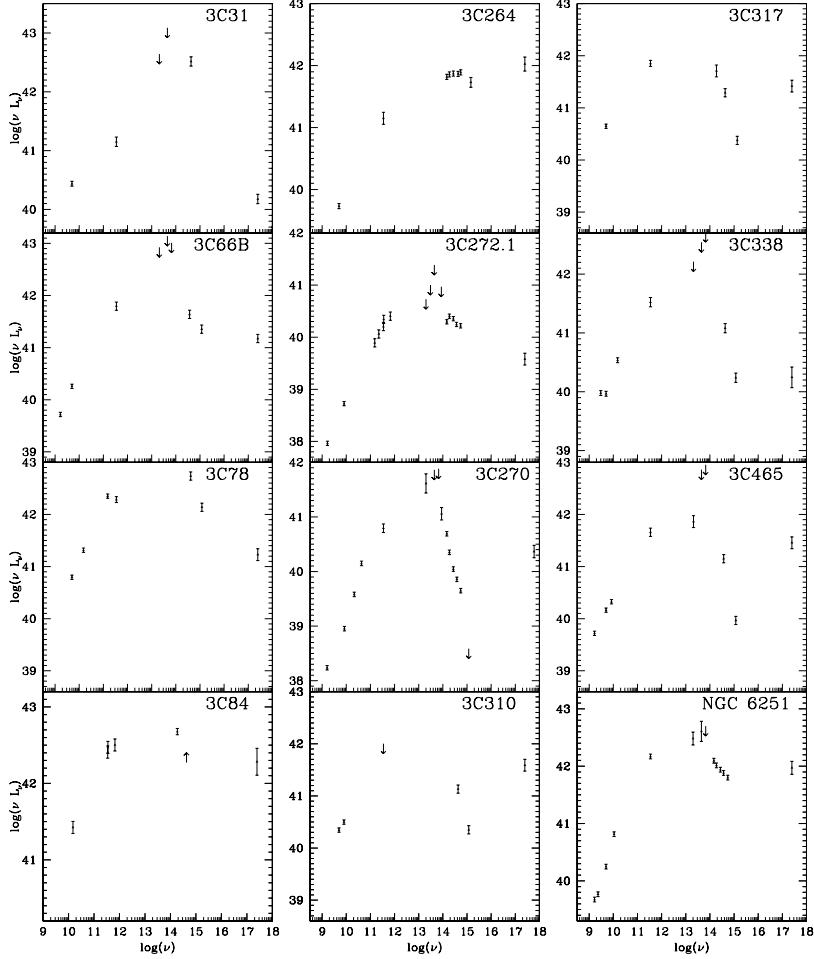
Fig. 3.— The SEDs of FR I nuclei for which we have many measured fluxes. See the accompanying tables for more information. 3C270(NGC 4261) and NGC 6251 have prominent edge-on dusty disks seen in optical HST images, whereas 3C264 has a face-on one. 3C272.1(M84) has a warped dusty disk. The steep drop in the SEDs of many of these galaxies between the near-infrared and UV is likely to be caused by extinction from dust. Excepting that of 3C264, all of these objects have SEDs resemble LBLs. We note that much of the scatter among these data is likely to be caused by intrinsic variability.

11
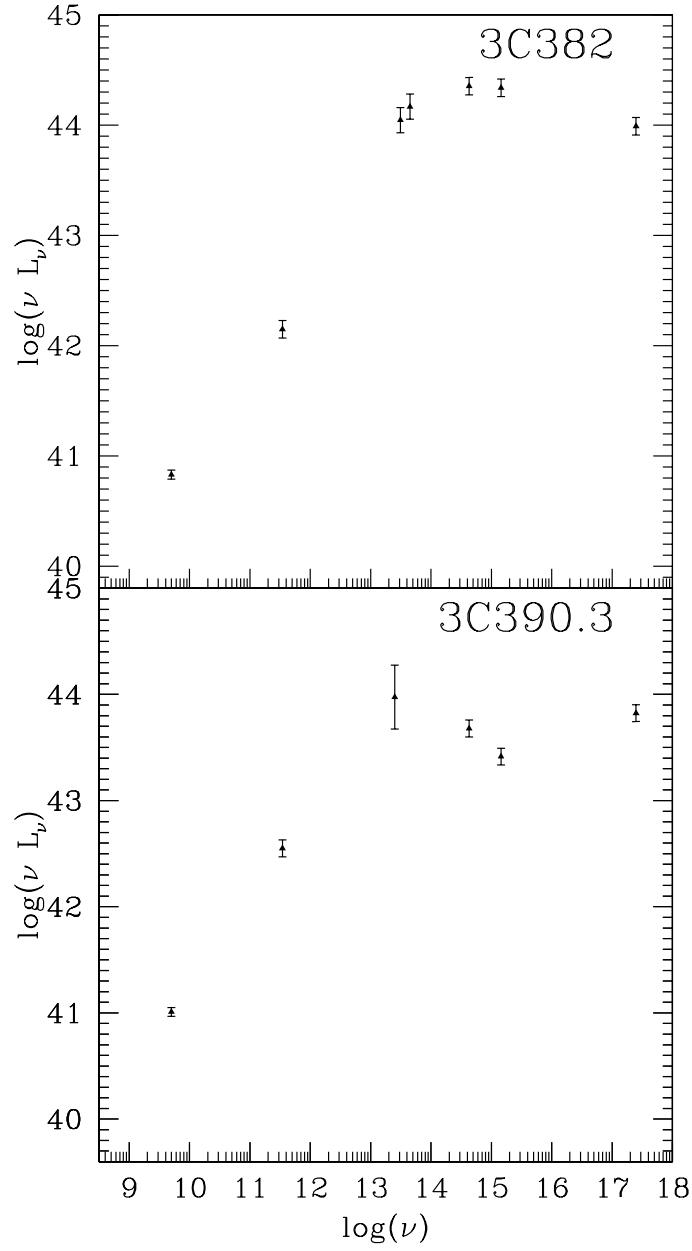
Fig. 4.— The SEDs of two FR II nuclei for which we have many measured fluxes. See the accompanying tables for more information. These two objects have high X-ray to submillimeter luminosity ratios suggesting that they could be similar to HBLs. From these SEDs, the synchrotron peaks are most likely to reside in the optical/UV region, intermediate between those of HBLs and LBLs particularly since extinction may have affected the optical/UV observations of 3C390.3. At an orientation angles pointed toward the observer, the spectrum would be harder pushing the expected location of the synchrotron peak toward the UV/Xray region. Therefor these objects could be candidate debeamed HBLs. The large X-ray to submillimeter luminosity ratios suggests that the high level of optical emission is not due to an extra component of emission (such as could be from a broad line region or accretion disk) but is a result of a higher energy peak of the synchrotron emission component.

TABLE 1
870μM BOLOMETRIC OBSERVATIONS

Galaxy	flux(mJy)	2σ limit (mJy)
3C31	75.29 ± 12.03	
3C35	-3.47 ± 15.88	< 31.75
3C35	-10.75 ± 12.89	< 25.77
3C66.0B	91.36 ± 12.43	
3C78	277.79 ± 46.24	
3C84	1259.84 ± 17.09	
3C88	71.49 ± 15.66	
3C98	-19.79 ± 12.10	< 24.21
3C111	4639.31 ± 29.31	
3C136.1	-5.58 ± 11.38	< 22.75
3C198	-0.66 ± 17.00	< 34.01
3C198	-5.65 ± 10.22	< 20.45
3C227	-31.88 ± 20.40	< 40.81
3C227	11.62 ± 10.32	< 20.65
3C236	47.93 ± 10.14	
3C264	47.35 ± 12.70	
3C270	166.71 ± 18.41	
3C272.1	133.98 ± 11.34	
3C274	1466.99 ± 17.34	
3C277.3	15.63 ± 10.63	< 21.26
3C293	47.88 ± 15.47	
3C296	48.07 ± 10.68	
3C305	28.57 ± 13.28	
3C310	22.62 ± 17.19	< 34.38
3C317	91.00 ± 12.22	
3C318.1	-5.99 ± 9.33	< 18.66
3C321	-2.40 ± 12.84	< 25.68
3C326	-20.46 ± 10.59	< 21.18
3C338	54.80 ± 12.14	
3C353	73.76 ± 10.11	
3C371	691.56 ± 22.79	
3C382	61.97 ± 11.93	
3C390.3	155.78 ± 13.32	
3C402	26.55 ± 13.13	
3C430	10.40 ± 16.14	< 32.28
3C452	33.18 ± 15.41	
3C465	76.20 ± 13.54	
NGC6251	423.30 ± 11.63	

TABLE 2

DERIVED SPECTRAL INDEXES

Galaxy	Luminosity@870μm	α_{sr}	α_{os}	α_{xs}
3C31.0	41.1	0.05	1.1	1.2
3C66.0B	41.4	0.16	1.0	1.1
3C78.0	42.2	0.29	0.9	$\cdots$
3C84.0	42.4	0.91	0.9	1.0
3C88.0	41.6	0.19	1.1	$\cdots$
3C111.0	43.8	-0.30	1.3	$\cdots$
3C236.0	42.5	0.13	$\cdots$	$\cdots$
3C264.0	41.0	0.34	0.8	0.9
3C270.0	40.7	0.14	1.4	1.1
3C272.1	39.9	0.07	1.0	1.1
3C274.0	41.2	0.23	1.1	1.1
3C293.0	41.8	0.17	$\cdots$	$\cdots$
3C296.0	41.2	0.11	1.3	1.0
3C305.0	41.5	0.01	$\cdots$	$\cdots$
3C317.0	41.8	0.34	1.2	1.1
3C338.0	41.5	0.15	1.1	1.2
NGC6251	42.2	0.16	1.1	1.0
3C353.0	41.6	0.10	$\cdots$	$\cdots$
3C371.0	43.0	0.22	0.8	$\cdots$
3C382.0	42.1	0.26	0.4	0.7
3C390.3	42.5	0.16	0.7	0.8
3C402.0	41.0	$\cdots$	0.9	$\cdots$
3C452.0	42.1	0.32	$\cdots$	$\cdots$
3C465.0	41.6	0.30	1.0	1.0

NOTE.—Spectral indexes for sources detected at 870μm. The log of the power in erg/s, estimated from the submillimeter flux, $\nu f_\nu 4\pi D^2$ is also listed. The distance D is estimated using the redshift and a Hubble constant of 75 km s^{-1} Mpc^{-1}. α_{sr} is the spectral index between the 5GHz core and submillimeter (870μm). The spectral indexes α_{os} and α_{xs} are those measured from the optical and submillimeter and x-ray and submillimeter flux densities, respectively. X-ray fluxes were taken from those compiled by Hardcastle & Worrall (1999, 2000); Sambruna et al. (1999); Trussoni et al. (2003); Chiaberge et al. (2003); Hardcastle et al. (2001), optical nuclear fluxes from those compiled by Chiaberge et al. (1999, 2000a, 2002b); Hardcastle & Worrall (2000).

TABLE 3

POINTS USED IN SPECTRAL ENERGY DISTRIBUTIONS

filter	$\lambda(\mu$m$)$	flux (mJy)	DATEOBS	Ref.
			NGC 6251	
ROSAT/HRI	1.2e-3	3.7e-4	1995 Jun 1	HW00
F547M	0.547	0.11	1996 Sep 13	$\cdots$
F814W	0.814	0.20	1996 Sep 13	$\cdots$
F110W	1.10	0.31	1998 Jun 7	$\cdots$
F160W	1.60	0.54	1998 Jun 7	$\cdots$
F205W	2.05	0.84	1998 Jun 7	$\cdots$
LW1	4.5	< 5	1996 Feb 26	$\cdots$
LW2	6.7	9	1996 Feb 26	$\cdots$
LW3	14.3	15	1996 Feb 26	$\cdots$
345GHz	870	423	2001 Feb 12	$\cdots$
10.7GHz	2.8e4	600	1983 Mar	J86
5.0GHz	6.0e4	350	1983 Mar	J86
2.3GHz	1.3e5	250	1983 Mar	J86
1.7GHz	1.8e5	280	1983 Mar	J86
			3C31	
Chandra	1.2e-3	1.1e-5	2000 Nov 6	T03
F702W	0.7	1.4	1995 Jan 19	$\cdots$
LW2	6.7	< 34	1997 Jan 31	$\cdots$
LW3	14.3	< 26	1997 Jan 31	$\cdots$
345GHz	870	75	2001 Feb 12	$\cdots$
5GHz	6e4	1000	1997 Feb 25	G01
1.7GHz	1.8e5	52	1997 Apr 9	X00
			3C66B	
Chandra	1.2e-3	3.0e-5	2000 Nov 20	H01
F25SRF2	0.253	9.6e-3	2000 Jul 13	C02b
F814W	0.702	0.06	1999 Jan 31	C02b
LW1	4.5	< 5	1997 Jan 26	$\cdots$
LW2	6.7	< 10	1997 Jan 26	$\cdots$
LW3	14.3	< 13	1997 Jan 26	$\cdots$
345GHz	870	91	2001 Feb 10	$\cdots$
5GHz	6e4	182	1993 Sep 12	G01
1.67GHz	1.8e5	157	1997 Apr 9	X00
			3C78 (NGC 1218)	

TABLE 3—*Continued*

filter	$\lambda(\mu\text{m})$	flux (mJy)	DATEOBS	Ref.
BeppoSAX	1.2e-3	3.4e-5	1997 Jan 7	T03
F25QTZ	0.248	5.7e-2	2000 Mar 15	C02b
F28X50LP	0.722	0.66	2000 Mar 15	C02b
345GHz	870	280	2001 Feb 11	$\cdots$
15GHz	2e4	689	1982 Jun 18	S86
5GHz	6e4	628	1982 Jun 18	S86
1.5GHz	2e3	752	1982 Jun 18	S86
3C84 (NGC 1275)				
ROSAT/HRI	1.2e-3	1.3e-3		HW00
F160W	1.6	4.3	1998 Mar 16	$\cdots$
F702W	0.70	>1	2000 Mar 3	$\cdots$
667GHz	450	810	1998 Jul 15	I01
350GHz	850	1420	1998 Jul 15	I01
345GHz	870	1260	2001 Feb 11	$\cdots$
15GHz	2e4	3000	1996	D98
3C264				
ROSAT/PSPC	1.2e-3	4.9e-4	1991 Nov 29	HW99
F25CN182	0.208	0.043	2000 Feb 12	T03
F547M	0.547	0.16	1996 May 19	$\cdots$
F702W	0.702	0.20	1994 Dec 24	$\cdots$
F110W	1.10	0.31	1998 May 12	$\cdots$
F160W	1.60	0.44	1998 May 12	$\cdots$
F205W	2.05	0.52	1998 May 12	$\cdots$
345GHz	870	47.3	2001 Feb 11	$\cdots$
5GHz	6e4	125	1993 Feb 25	L97
3C270 (NGC 4261)				
Chandra	2e-4	3.6e-5	2000 May 6	C03
F25SRF2	0.253	$<$2e-4	2000 Mar 5	C02b
F547M	0.547	7.6e-3	1994 Dec 13	$\cdots$
F791M	0.791	1.8e-2	1994 Dec 13	$\cdots$
F110W	1.10	3.8e-2	1998 Apr 23	$\cdots$
F160W	1.60	0.11	1998 Apr 23	$\cdots$
F205W	2.05	0.31	1998 Apr 23	$\cdots$
L	3.4	1.2	2000 Mar 21	$\cdots$

TABLE 3—*Continued*

filter	$\lambda(\mu m)$	flux (mJy)	DATEOBS	Ref.
LW1	4.5	< 7	1996 Jul 2	$\cdots$
LW2	6.7	< 10	1996 Jul 2	$\cdots$
LW3	14.3	19	1996 Jul 2	$\cdots$
345GHz	870	167	2001 Feb 11	$\cdots$
43GHz	0.7e4	305	1997 Sep 7	J00
22GHz	1.4e4	165	1997 Sep 7	J00
8.4GHz	3.6e4	100	1995 Apr 1	J97
1.6GHz	1.87e5	100	1995 Apr 1	J97

3C272.1 (M84,NGC 4374)

filter	$\lambda(\mu m)$	flux (mJy)	DATEOBS	Ref.
Chandra	1.2e-3	4.4e-5	2000 May 19	T03
F547M	0.555	8.83e-2	1996 Mar 4	B00
F814W	0.814	1.38e-1	1996 Mar 4	B00
F110W	1.10	0.24	1998 Jul 13	B00
F160W	1.60	0.39	1998 Jul 13	B00
F205W	2.05	0.39	1998 Jul 13	B00
L	3.45	< 2	2000 Mar 22	$\cdots$
LW2	6.7	< 10	1996 Jul 5	$\cdots$
LW7	9.7	< 6	1996 Jul 5	$\cdots$
LW3	14.3	< 5	1996 Jul 5	$\cdots$
677GHz	450	110	1999 Mar 19	L00
350GHz	850	180	1999 Mar 19	L00
345GHz	870	134	2001 Feb 10	$\cdots$
221GHz	1350	150	1999 Feb 14	L00
146GHz	2000	150	1999 Mar 19	L00
8.09GHz	3.71e4	190	1978	J81
1.67GHz	1.80e5	160	1978	J81

3C310

filter	$\lambda(\mu m)$	flux (mJy)	DATEOBS	Ref.
ROSAT/HRI	1.2e-3	2.8e-5	1996 Jan 30	HW99
F25SRF2	0.253	3.41e-4	2000 Jun 10	C02b
F702W	0.70	5.7e-3	1994 Sep 12	C02b
345GHz	870	< 34	2001 Feb 10	$\cdots$
5GHz	6e4	80	1973 May	G88

3C317

filter	$\lambda(\mu m)$	flux (mJy)	DATEOBS	Ref.
ROSAT/PSPC	1.2e-3	4.6e-5	2000 Sep 3	T03
F210M	0.221	7.7e-4	1994 Mar 5	C02b

TABLE 3—*Continued*

filter	$\lambda(\mu m)$	flux (mJy)	DATEOBS	Ref.
F702W	0.70	2.0e-2	1994 Mar 5	C02b
F160W	1.6	0.12	1998	T03
345GHz	870	91	2001 Feb 10	$\cdots$
5GHz	6e4	391	1989 Sep	M93
3C338 (NGC 6166)				
Chandra	1.2e-3	4e-6	1999 Dec 11	T03
F25SRF2	0.253	8.3e-4	2000 Jun 4	C02b
F702W	0.70	1.6e-2	1994 Sep 9	C02b
LW1	4.5	< 3	1996 Mar 2	$\cdots$
LW2	6.7	< 3	1996 Mar 2	$\cdots$
LW3	14.3	< 3	1996 Mar 2	$\cdots$
345GHz	870	55	2001 Feb 11	$\cdots$
8.4GHz	1e4	180	1990	G98
5GHz	6e4	105	1980 May 4	G01
1.4GHz	1e5	130	1990	G98
3C382				
ROSAT/HRI	1.2e-3	5.95e-3	1992 Mar 13	HW99
F25CN182	0.2078	2.3	2000 Feb 23	C02b
F702W	0.700	8.0	1994 Jun 25	C02b
LW2	6.7	50	1997 Feb 16	$\cdots$
LW7	9.6	54	1996 Feb 16	$\cdots$
345GHz	870	62	2001 Feb 11	$\cdots$
5GHz	6e4	206	1990 Nov	G01
3C390.3				
ROSAT/HRI	1.2e-3	4.3e-3	1995	HW99
F25CN182	0.208	2.9e-1	2000 Aug 10	C02b
F702W	0.70	1.8	1994 Sep 20	C02b
345GHz	870	166	2001 Feb 12	$\cdots$
5GHz	6e4	330		G88
3C465				
ROSAT/HRI	1.2e-3	6.6e-5	1995 Jan 12	HW99
F25SRF2	0.253	4.5e-4	2000 May 25	C02b
F702W	0.70	5.7e-2	2000 Jul 3	C02

TABLE 3—*Continued*

filter	$\lambda(\mu m)$	flux (mJy)	DATEOBS	Ref.
LW1	4.5	5.9	1996 Dec 15	$\cdots$
LW2	6.7	< 4.7	1996 Dec 15	$\cdots$
LW3	14.3	2	1996 Dec 15	$\cdots$
345GHz	870	76	2001 Feb 10	$\cdots$
8.4GHz	3.6e4	146	1992 Jan	V95
5GHz	6e4	168	1992 Mar	V95
1.7GHz	2e4	181	1992 Jan	V95

NOTE.—F25SRF2, F25QTZ, F25CN182, F28X50LP filters refer to STIS/HST UV and optical measurements. The F110W, F160W, F205W filters refer to those from NICMOS (on board HST) $1 - 2\mu m$. F547M, F702W, F814W filters refer to optical WFPC2/HST measurements. The LW1, LW2, LW3, LW7 filters refer to $4 - 15\mu m$ data from ISOCAM images. L band measurements are based on ground based images obtained by us at the IRTF. The date of the observations are also listed.

References. — B00 (Bower et al. 2000); C02b (Chiaberge et al. 2002b); C03 (Chiaberge et al. 2003); D98 VLBI core (Dhawan et al. 1998); G01 VLBI (Giovannini et al. 2001); G98 Giovannini et al. (1998); G88 Giovannini et al. (1988); H01 (Hardcastle et al. 2001); HW00 mostly ROSAT (Hardcastle & Worrall 2000); HW99 mostly ROSAT (Hardcastle & Worrall 1999); I01 SCUBA (Irwin et al. 2001); J81 VLBI (Jones et al. 1981) J86 VLBI (Jones 1986); J97 VLBA (Jones & Wehrle 1997); J00 VLBA (Jones et al. 2000); L00 SCUBA (Leeuw et al. 2000); L97 VLBI (Lara et al. 1997); M93 (Morganti et al. 1993); S86 VLA and VLBI (Saikia et al. 1986); T03 (Trussoni et al. 2003); V95 VLBI (Venturi et al. 1995); X00 VLBA (Xu et al. 2000). When no reference is given we measured the fluxes ourselves using procedures described by Alonso-Herrero et al. (2003).